

Changes of Variability in Response to Increasing Greenhouse Gases. Part I: Temperature

R. J. STOUFFER AND R. T. WETHERALD

NOAA/Geophysical Fluid Dynamics Laboratory, Princeton, New Jersey

(Manuscript received 6 March 2006, in final form 9 March 2007)

ABSTRACT

This study documents the temperature variance change in two different versions of a coupled ocean–atmosphere general circulation model forced with estimates of future increases of greenhouse gas (GHG) and aerosol concentrations. The variance changes are examined using an ensemble of 8 transient integrations for the older model version and 10 transient integrations for the newer one. Monthly and annual data are used to compute the mean and variance changes. Emphasis is placed upon computing and analyzing the variance changes for the middle of the twenty-first century and compared with those found in a control integration.

The large-scale variance of lower-tropospheric temperature (including surface air temperature) generally decreases in high latitudes particularly during fall due to a delayed onset of sea ice as the climate warms. Sea ice acts to insulate the atmosphere from the much larger heat capacity of the ocean. Therefore, the near-surface temperature variance tends to be larger over the sea ice–covered regions, than the nearby ice-free regions. The near-surface temperature variance also decreases during the winter and spring due to a general reduction in the extent of sea ice during winter and spring.

Changes in storminess were also examined and were found to have relatively little effect upon the reduction of temperature variance. Generally small changes of surface air temperature variance occurred in low and midlatitudes over both land and oceanic areas year-round. An exception to this was a general reduction of variance in the equatorial Pacific Ocean for the newer model. Small increases in the surface air temperature variance occur in mid- to high latitudes during the summer months, suggesting the possibility of more frequent and longer-lasting heat waves in response to increasing GHGs.

1. Introduction

In earlier papers, the mean climate response to changes in the earth's radiative forcing on a wide range of variables and time scales is described in detail [e.g., Manabe et al. 1991; Intergovernmental Panel on Climate Change (IPCC) Working Group I Reports, see Houghton et al. 1990, 1996, 2001]. However, it is also of interest to examine changes in variability in addition to the changes in the mean climate state. This is particularly important when one wishes to discuss changes in the occurrence of extreme events in response to increasing greenhouse gases (GHGs) in the atmosphere. These extreme events include floods, droughts, storm frequency, hot and cold spells, etc. For the most part, previous investigations of variability change resulting

from increasing GHGs have focused on specific regions or phenomena such as El Niño–Southern Oscillation (ENSO), Arctic Oscillation (AO), storm tracks, and frequency, etc. (e.g., Mearns 1993; Mearns et al. 1995; Rind et al. 1989; Katz and Brown 1992; Zwiers and Kharin 1998; Meehl and Tebaldi 2004; Meehl et al. 2006).

Other recent studies have concentrated on the interaction of time mean changes versus variability of climate change. For example, the study by Raisanen (2002) employed an ensemble of 19 different coupled atmosphere–ocean models and noted that although there were changes in interannual monthly mean temperature and precipitation variability in response to greenhouse warming, these were found to be relatively small in comparison to the time mean changes. A similar conclusion was reached in a later study by Hunt and Elliot (2004). Their study also considered variations of droughts, extreme rain events over Australia, and cold outbreaks over North America under greenhouse warming conditions.

Corresponding author address: Ronald J. Stouffer, NOAA/GFDL, Princeton, NJ 08542.
E-mail: ronald.stouffer@noaa.gov

This study takes a more broad-based view in its investigation. In particular, we examine changes in the annual and seasonal mean temperature variability over the entire global domain to determine whether or not there are systematic changes in the variance. We seek to investigate the causes of these changes. Naturally, some of the variance changes we see will be related to changes in the phenomena mentioned above. However, we believe there are also large-scale changes in the variance fields that are closely related to changes in the mean state of the climate system. If the uncertainty associated with the changes in the mean state are low, then it is likely that the uncertainty associated with the related variance changes would also be low. This paper discusses only the large-scale temperature variability changes; hydrologic variability changes will be investigated in a companion paper.

One of the main difficulties in this type of analysis is the computation of variance when the mean climate state is changing. Here we use a statistical method proposed by Vinnikov and Robock (2002, hereafter called the VR method) to compute the variances. The VR method consists of fitting a higher-order polynomial to the input time series. Anomalies are then computed as deviations from that polynomial. By definition, the anomalies squared are the variance time series. While relatively simple, the VR scheme has the capability of determining a unique time series of variances and to cleanly separate the changes in the mean climate from the changes in variance. See the appendix for more details.

2. Model description

The two models used in this investigation are an older generation model that will be referred to as the R30 Manabe Climate Model (MCM; Delworth et al. 2002) and a newer version called climate model version 2.1 (CM2.1; Delworth et al. 2006). Since both models have been extensively described in prior publications, we will simply highlight a few attributes here. For more details of the two models, the reader is encouraged to investigate the two Delworth et al. papers and references therein.

The R30 model was developed in the late 1980s and uses relatively simple physical subgrid-scale parameterizations. The results obtained from this model were used in the previous IPCC and other national and international climate reports and assessments (Delworth et al. 2002). The CM2.1 model is newly developed, using newer numerical techniques for advection and much more complex physical parameterizations for subgrid-scale processes (Delworth et al. 2006). It also includes many new features not found in the early R30

model such as the ability to simulate the climatic effect of many types of aerosols and the inclusion of diurnal variation. The CM2.1 results are being used in the 2007 Fourth IPCC Assessment Report (AR4) and will likely be part of many future assessments.

The R30 atmospheric transform grid, 2.25° latitude by 3.75° longitude, is slightly coarser than the 2° latitude by 2.5° longitude CM2.1 atmospheric grid. The atmospheric component of CM2.1 uses about twice as many vertical levels—24 levels as compared to 14 levels in the R30 model. The oceanic R30 grid is a 2° grid with 18 vertical levels, while the CM2.1 oceanic grid is 1° with higher resolution in the Tropics and has 50 vertical levels.

In the R30 model, surface hydrology and precipitation are computed using a 15-cm “bucket” and the “moist convective adjustment” scheme, respectively (Manabe 1969). Runoff is computed when the amount of liquid water exceeds the field capacity of the bucket. Cloud cover is a function of relative humidity only. No heat storage is allowed in the land surface.

The CM2.1 land surface component is described in Milly and Shmakin (2002) and is similar in complexity to the Manabe bucket scheme, especially for hydrological processes. However, an additional feature is the use of a global distribution of field capacities derived from vegetation- and soil-type datasets which replaces the uniform 15-cm field capacity used in the R30 model. The CM2.1 land surface component allows heat storage over the continents.

Precipitation in CM2.1 is computed according to the Relaxed Arakawa–Schubert formulation of Moorthi and Suarez (1992). In general, large-scale clouds and cloud microphysics are determined according to Rotstayn (1997), whereas cloud amount is forecast-based upon the scheme given by Tiedtke (1993).

In this study, sea ice changes are important. In the R30 model, the sea ice moves with the ocean currents. There are no leads within a given grid cell. If sea ice exists, it is assumed to completely cover the grid cell. In CM2.1, the ice scheme is more complicated (Delworth et al. 2006). Ice dynamics are included. Ice moves in response to the wind and ocean stresses taking into account the internal ice forces. Snow is allowed to accumulate on the ice and there are two ice layers for the thermodynamical computation. In a given grid cell in CM2.1, there can be leads and up to five thicknesses of the sea ice.

The R30 model uses flux adjustments to limit climate drift and help maintain a stable control integration climate. These flux adjustments are computed in integrations that occur before the model is coupled and they are identical in the control and perturbation integra-

tions. In CM2.1, no flux adjustments are used. In summary, the R30 is a relatively simple, fast-running climate model, which was state of the art in the early 1990s. CM2.1 is a much more complex model and represents the present-day state of the art.

The experimental procedure used to initialize and integrate the R30 model is identical to that described by Wetherald and Manabe (2002). We analyze their ensemble of eight transient integrations and corresponding control integrations. The control integrations, where the radiative forcing is held constant at 1860 values, are about 900 yr in length. To obtain the projections of the future climate changes, an eight-member ensemble is radiatively forced by increasing equivalent GHG concentrations and sulfate aerosols over the period of 1860–2090. From 1860 to 1990, historical estimates of the changes in radiative forcing are used, including the observed increases in GHG and sulfate aerosols [see GHG and sulfate (GS) attributes in Table 4 of Delworth et al. 2002]. All eight integrations started from different points (approximately 40 yr apart) in the long preindustrial control run. From 1990 to 2090, the IS92a scenario of the IPCC (Houghton et al. 1990) was used.

For CM2.1, initialization and radiative forcing are quite different from those used for the R30 model. This is partly due to the fact that CM2.1 does not need to use flux adjustments to maintain a stable control climate and partly because of the more complex radiative forcings used to drive the model. The control 1860 integration is obtained using the method described in Stouffer et al. (2004). In this integration, the radiative forcing is held constant at 1860 conditions and time integrated for more than 1000 model years. Again, to obtain the future projections of climate change, perturbation integrations started from different periods in the 1860 control integration. The perturbation integrations from 1860 to 2000 use estimates of the historical changes in the radiative forcing. The CM2.1 integrations include many additional forcing agents not used in the R30 model integrations such as volcanic aerosols, observed solar irradiance changes, and land surface changes over that time period. For the CM2.1 model, the control integration climate drift is larger than in the R30 model. Therefore, a 100-yr period was selected that corresponded in time with the analysis period (years 2035–65) used for the transient experiments.

A number of different future radiative forcing scenarios were run using CM2.1 in support of the IPCC AR4. An ensemble of 10 integrations using the Special Report on Emissions Scenarios (SRES) A1B scenario (see Nakicenovic et al. 2000 for a description of this scenario) is analyzed in the same manner as the results

from the R30 model. In this case, all 10 members started from year 1990 of the CM2.1 historical run described above, using small perturbations in the initial conditions to obtain the different ensemble members.

It should be noted here that while using different radiative forcing agents, the historical radiative forcings (1860 to the present day) used to drive the two models are similar (IPCC report, Houghton et al. 2001). As for the future scenarios, the IS92a scenario used in the R30 runs has been replaced by a newer, more realistic forcing scenario SRES A1B (see above). The radiative forcing in the IS92a scenario is somewhat larger than the SRES A1B scenario. All other factors being equal, one would expect a larger climate response in the R30 results than is found in the CM2.1 results, because of the larger radiative forcing.

The model data analyzed in this study consists of both yearly and monthly mean time series from the ensemble of 8 transient experiments from the R30 model and 10 transient experiments from the CM2.1 model plus their respective control runs. The analysis presented here focuses on a time period in the middle of this century (2035–65). The response is presented as differences from preindustrial control integrations. We chose the 2035–65 calendar year time period because it coincides with the time period analyzed in the Wetherald and Manabe (2002) study. If we had chosen a later time period, the amplitude of the changes would have been somewhat larger and possibly more statistically significant but the patterns would have remained similar, assuming the sampling issues are small.

3. Analysis and results

The annual mean surface air temperature (SAT) difference is maximum in northern polar regions and minimum in tropical latitudes for both the R30 and CM2.1 models. There is a local SAT difference minimum in the northern North Atlantic Ocean and a secondary weak minimum near 60°S (Figs. 1a,c). This pattern is very similar to earlier studies (Manabe et al. 1991; Cubasch et al. 2001). The maximum SAT increase in the northern polar latitudes, and to some extent in the southern polar region, is enhanced by snow cover–albedo feedback, a mechanism that is extensively discussed in Manabe and Wetherald (1975).

The patterns of the SAT variance changes (Figs. 1b,d) are very different from the changes in the mean fields (Figs. 1a,c). The SAT variability generally decreases in both models in the northern and southern polar oceanic regions, near the sea ice margin. In both models, there are small variance changes in low latitudes. In the CM2.1 results, there is a large increase in SAT variance over near the North Pole.

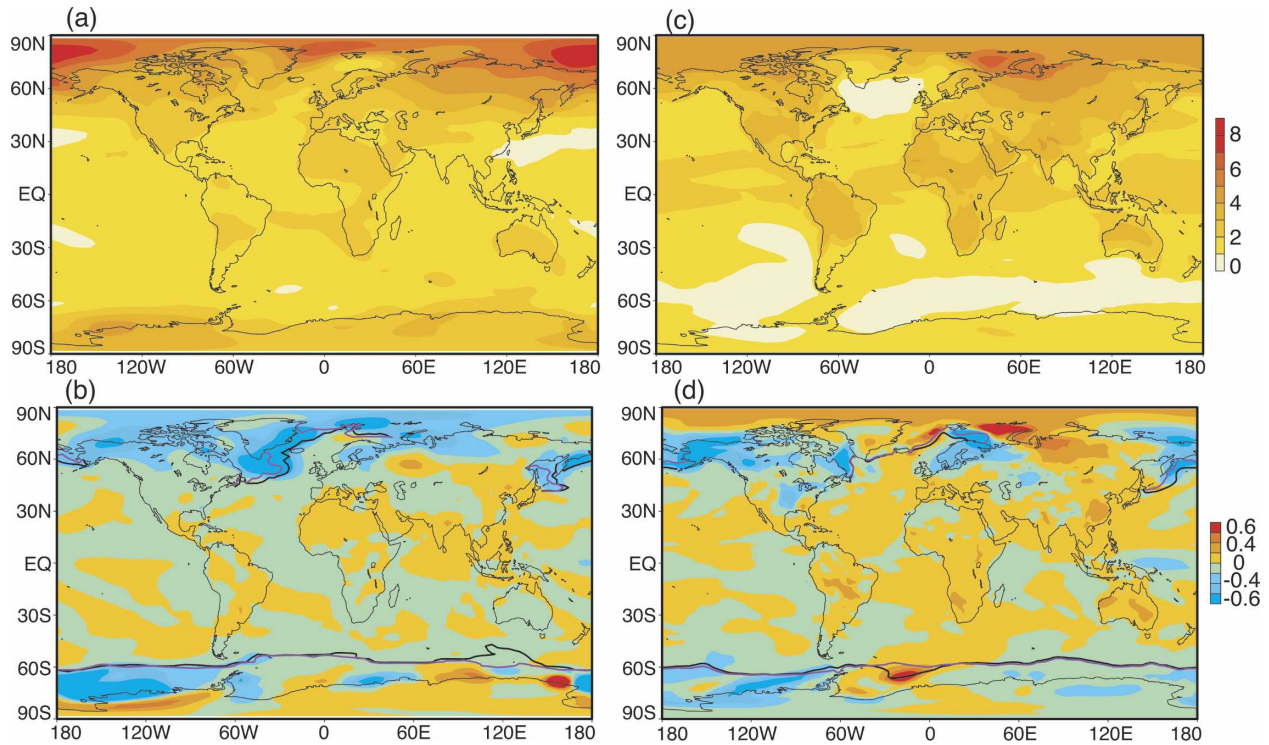


FIG. 1. Horizontal distribution of (a) annually averaged SAT difference and (b) SAT variance differences for the R30 model. Horizontal distributions of (c) annually averaged SAT difference and (d) SAT variance differences for the CM2.1 model. Here the variance changes are computed for each model ensemble member and averaged. Units are (a), (c) $^{\circ}\text{C}$ and (b), (d) $^{\circ}\text{C}^2$. Control integration data were obtained from the 900 yr of the R30 model and 100 yr of the CM2.1 model integrations. Transient integration data for years 2035–65 from each of the ensemble members are used, yielding differences from the control centered at the year 2050 or the middle of the twenty-first century. Thick, dark lines signify boundaries of sea ice for the control runs; the maroon lines signify sea ice boundaries around year 2050 from one of the ensemble experiments. The boundaries represent values larger than 1-cm thickness in the annual average.

Additional investigation indicates that the pattern of SAT variance decrease in high latitudes is associated with the change in the latitude of the edge of the sea ice pack or reductions in the sea ice thickness as discussed below. By 2050 in these integrations, the sea ice generally becomes much thinner and the ice edge moves farther poleward (Figs. 1b,d). By 2050, the sea ice is completely absent in some locations and in some seasons where it is present in the control integration.

In the control integrations of both models due to the smaller heat capacity of the underlying surface, the SAT variance over relatively thick sea ice is larger than over a thinner ice layer or the open ocean. Sea ice isolates the overlying atmosphere from the ocean below (Manabe and Stouffer 1979). Where the sea ice is relatively thick, the SAT variability in the control integrations is generally larger. In fact in places where the sea ice is thick enough, the magnitude of the SAT variance is similar to that found over the adjacent land regions.

In the transient integrations, the climate warms. In response, the sea ice becomes thinner and the ice edge

retreats poleward. This allows more interactions between the atmosphere and ocean, leading to SAT variance decreases. This association of the SAT variance changes with the changes in the underlying surface is also found in Kharin and Zwiers (2005).

Comparing the amplitude of the SAT mean and variance changes between R30 and CM2.1 (Figs. 1b,d), it is apparent that the changes are smaller for the CM2.1 results than found in the R30 model results. At least part of the differences in the response is due to the somewhat smaller radiative forcing in the CM2.1 integrations as noted earlier. A second reason for a smaller response in CM2.1 is its larger, and likely more realistic, oceanic heat uptake in the transient integrations (Russell et al. 2006; Stouffer et al. 2006b).

Another way to examine the changes of variability is by plotting the ratio of the variance obtained from the transient and control experiments. The advantage of this approach is that the ratio is directly related to the F statistical significance test. In all variance ratio plots shown here, the end member colors in the shading rep-

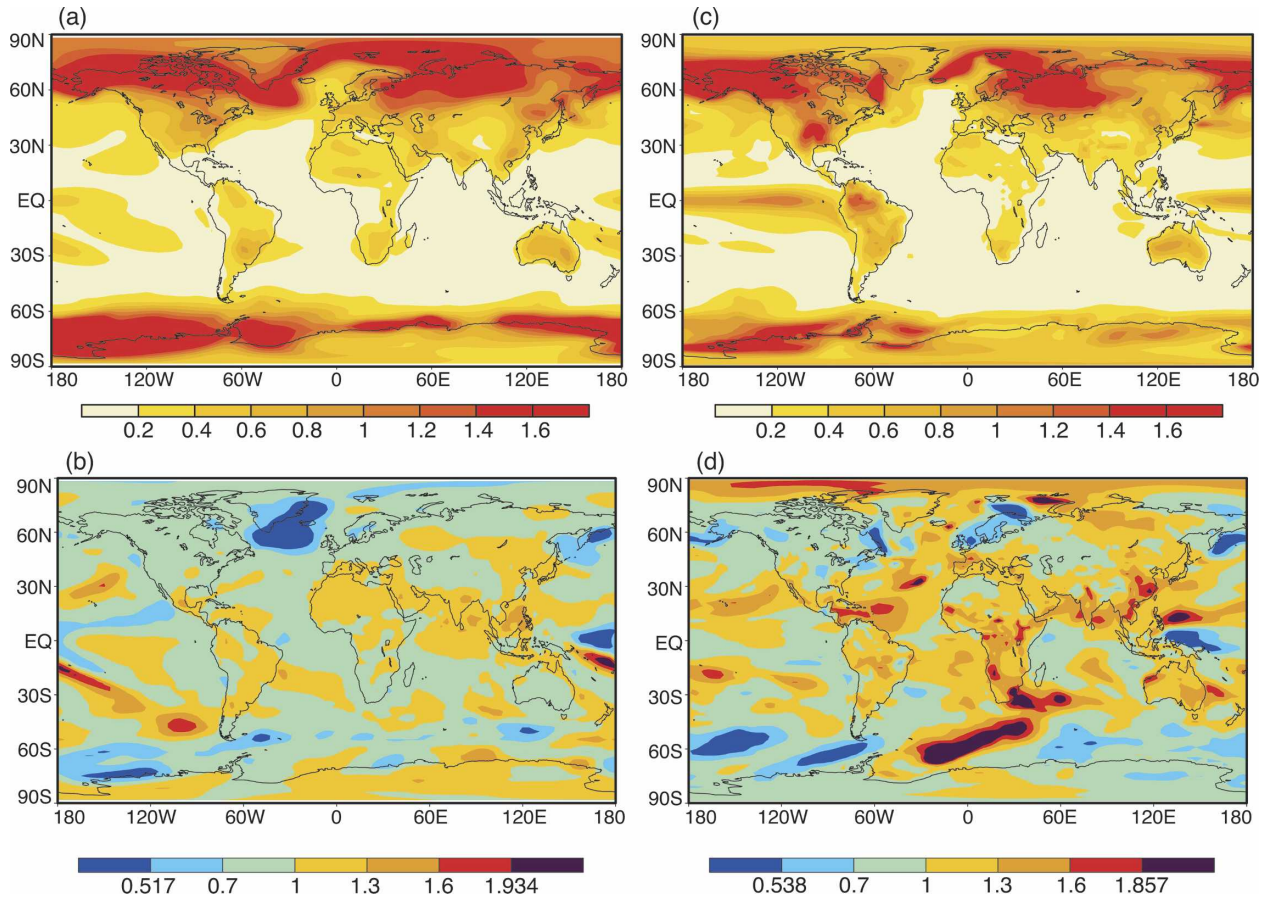


FIG. 2. Horizontal distribution of (a) annually averaged SAT variance from the R30 control experiment, (b) R30 SAT variance ratio, (c) annually averaged SAT variance from the CM2.1 control experiment, and (d) CM2.1 SAT variance ratio. Here, the variances are computed for each model ensemble member and averaged. Control integration and transient data used are from the same time periods as in Fig. 1. Variance ratios are defined as the variance obtained from the transient experiments divided by the respective control variances. Ratios less than 1 denote variance decreases in transient integrations whereas ratios greater than 1 denote variance increases. The degrees of freedom are 29 for both model control runs; 7 and 9 for the transient R30 and CM2.1 runs, respectively. These are conservative estimates for the degrees of freedom. The corresponding critical F values for decreases and increases of variance ratio (two-tailed test) at the 90% confidence level are 0.517 and 1.934 for the R30 results and 0.538 and 1.857 for CM2.1, respectively (end-member shades). Units are (a), (c) $^{\circ}\text{C}^2$ and (b), (d) dimensionless.

resent the 90% confidence level for the statistical significance of the changes. To estimate this confidence level, we assume a conservative number of degrees of freedom. For the control integrations, we assume the degrees of freedom are the number of non-overlapping segments in time in the integration. For the transient changes, we use the number of ensemble members.

A common feature of both model control distributions is that the SAT variability is largest in the polar regions and smallest in the Tropics (Figs. 2a,c). In CM2.1 (Fig. 2c), there is also a relative maximum in the SAT variance in the equatorial tropical Pacific. These patterns are related to the modes of variability found in the coupled system and to the heat capacity of the un-

derlying surface. Here it is seen that the variability of SAT for CM2.1 in high latitudes is smaller than that for the R30 results, which probably is related to the differences in the sea ice formulation. The R30 sea ice scheme does not allow leads within a grid box, while leads are simulated in CM2.1. In the R30 using the no-lead sea ice scheme, the variability over sea ice-covered regions is more like the variability found over land areas, leading to larger variability in these regions as discussed below.

Figures 2b,d show the ratio of SAT variance of the transient experiments to the variance of their respective control runs for both the R30 and CM2.1 results. The pattern of the ratios is clearly related to the pattern of the variance differences shown in Figs. 1b,d, although

the relationship between changes of variance and sea ice margins is no longer obvious.

Due to the small sample size, very few of the changes seen in Fig. 2 are statistically significant at the 90% level. However, regions that are statistically significant at the 90% confidence level for the R30 model include the following: southeast of Greenland, off the southeastern coast of Asia, and just north of Antarctica located between 180° and 100°W. All three regions are places where the retreat of sea ice and a corresponding decrease of SAT variability occurred. In CM2.1 the statistically significant variance change regions include the following: southwest of Greenland, the Bering Sea, off the northwestern coast of Europe, and approximately the same general area north of Antarctica as in the R30 model. Again, these regions correspond to areas where sea ice retreated and SAT variability decreased.

Finally, there is an increase in SAT variability for CM2.1 just north of the Antarctic continent centered approximately at 0° longitude. This is explained by an increase of sea ice in this region (see Fig. 1d). An increase in sea ice extent is the opposite of what occurred in most of the other ice margin regions. Therefore, the converse argument to the sea ice margin retreat noted above is also invoked here as the explanation of these changes: an extension of the sea ice boundary results in a local increase of SAT variability. This highlights the importance of the changes in the underlying surface in understanding the SAT variance changes.

Sea ice increases are also associated with small increases in SAT variance in the Labrador and Norwegian Seas and south of Greenland in the CM2.1 transient results. These regions are known to have a large impact in various important climatic processes such as the ocean's thermohaline circulation. For example in the Norwegian Sea, the deep ocean sinking was reduced by approximately 10%–30%, depending upon location in these transient integrations (Delworth et al. 2006). In spite of the general warming, these regions are cold enough in the transient integration to allow more sea ice to form during late winter due to the reduction in the oceanic convection (Stouffer et al. 2006a). The sea ice helps insulate the atmosphere from the ocean, resulting in a smaller effective heat capacity at the surface. This leads to a small increase in the SAT variance.

The increase in CM2.1 SAT variance changes in the Barents Sea is more complicated. Not all the ensemble members show an increase in the SAT variance in this region. The Barents Sea is rarely a site for deep-water formation in the CM2.1 control integration, so that the local surface heat flux anomalies are not well correlated to the SAT anomalies (Fig. 3, black dots). The sea ice present in the control, especially during the winter and

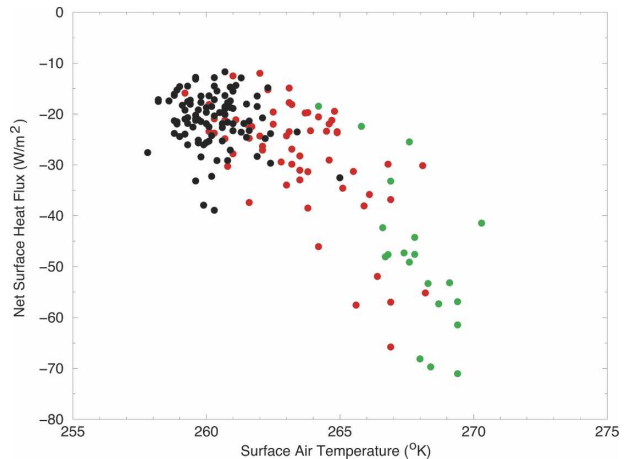


FIG. 3. Scatterplot of annually averaged SAT and net surface heat flux (positive into the ocean) in the Barents Sea region for the control integration (black dots, 100 yr) and one member of the ensemble of transient integrations for the CM2.1 model (red dots first 60 yr, green dots last 20 yr). The net surface heat flux is the sum of short- and longwave radiative fluxes as well as sensible and latent heat fluxes at the ocean surface in ice-free regions and the flux through the ice in ice-covered regions. Units are in K for SAT and W m^{-2} for the net surface heat flux.

spring, insulates the atmosphere from the large heat capacity of the ocean mixed layer. The surface SAT anomalies are therefore the result of atmospheric processes, and the variance can be similar to land areas as discussed above.

In the CM2.1 transient integrations, the frequency of deep-water formation increases in most of the ensemble members. During periods of deep-water formation and due to the general warming in response to the increasing GHGs, sea ice in the Barents Sea region is greatly reduced and the SAT is higher and more closely coupled to the SST and therefore to the ocean mixed layer (Fig. 3, green dots). By the end of the transient integrations, the SAT anomalies become highly correlated to the surface heat fluxes anomalies (Fig. 3), suggesting that the ocean is driving the SAT variability in this region. This region's response is therefore quite different than what is seen in other places where the sea ice disappears as the radiative forcing increases. In those areas, the large heat capacity of the oceanic mixed dampens the SAT anomalies making the SAT variance smaller in the warmer world.

In the R30 integrations, the increases of SAT variance (and the associated frequency of oceanic convection) did not occur. The physical mechanism involved in producing the CM2.1 variance changes seems sensitive to model formulation and potentially the Barents Sea simulation found in the control integration. In summary, it is unclear if the increased SAT over the Bar-

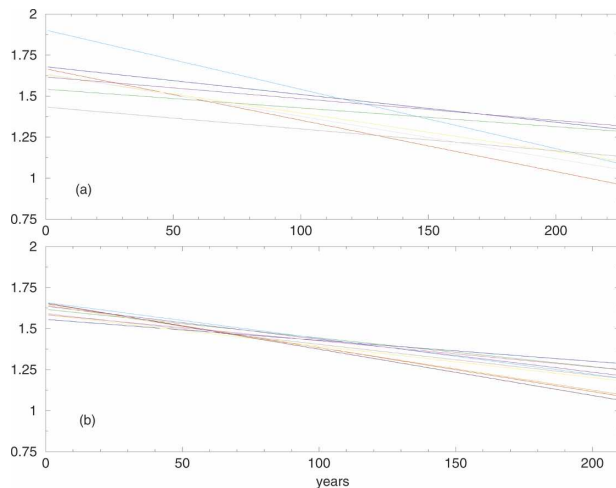


FIG. 4. Trend in the variance time series for each separate transient experiment as computed by linear least squares from Eq. (3) and integrated over the zonal belt of 60° – 90° N latitude. Results are shown for (a) the R30 model taken over 225 model years and (b) the CM2.1 model taken over 60 model years. The slope of each line is given by the coefficient b_2 [see Eq. (A3) in the appendix] for each case. Units are in $^{\circ}\text{C}^2$.

ents Sea and associated oceanic variability in CM2.1 is realistic. It would be interesting to evaluate this response in other AOGCMs.

One method to qualitatively demonstrate the viability of the high-latitude SAT changes is to examine the consistency of the general reduction of variance in high northern latitudes among the ensemble members (Fig. 4). This figure shows the trend computed over the integrated 60° – 90° N latitude from the variance time series [Eq. (A3) in the appendix] for each of the transient integrations. Here it is seen that all 8 of the R30 integrations (Fig. 4a) and all 10 CM2.1 integrations (Fig. 4b) exhibit a negative slope to some degree. This indicates that the variance reduction in the high northern latitudes is a typical feature in all 18 integrations.

The maximum increase of annual mean lower-tropospheric and surface temperature is found in the northern polar region with a secondary maximum located in the upper troposphere in tropical latitudes (Fig. 5a). The net result of the near-surface polar temperature increase is to reduce the lower-tropospheric meridional temperature gradient in the NH. Aloft, the increase of upper-tropospheric temperature in the Tropics and subtropics acts to increase the meridional temperature gradient in both hemispheres. The surface air temperature in the southern polar region has a small increase, due to the large oceanic mixing present around Antarctica, which inhibits the temperature response over very long time periods (Manabe et al. 1991; Stouffer 2004). The overall pattern of vertical tempera-

ture change has been noted in other earlier studies (Manabe and Wetherald 1975, 1980; Cubasch et al. 2001).

There is a general decrease of variability in the lower troposphere and at the surface in the northern and southern polar regions of both the R30 and CM2.1 models (Figs. 5b,c, respectively). Note that there is a maximum decrease that occurs at or near the surface in both models in the latitude zones of 50° – 75° N and 50° – 75° S, which is again an indicator that this decrease is due to the thinning and disappearance of sea ice at its boundary, which was mentioned above. The lower-troposphere variance changes are consistent with the results shown for the SAT (Figs. 1b,d and 2b,d) and, again, the magnitude of the variance change is less for the CM2.1 model than for R30 in the northern polar regions. In the mid- and upper troposphere there are, generally, small reductions in the variability for both models with a general increase in the variability in CM2.1 in the Tropics. In the distributions (Figs. 5b,c), no region is statistically significant at the 90% confidence level although the R30 changes of variability in the northern polar region come close to this limit.

Similar changes in the vertical structure of the temperature variance were noted in an earlier study by Manabe and Wetherald (1980). In that study, the decrease in temperature variance (their Fig. 7b) was attributed mainly to a decrease in the meridional temperature gradient. However, the current analysis suggests that retreat of the sea ice edge and sea ice thinning are more important factors in reducing the temperature variance in high latitudes.

The monthly mean SAT difference for both the R30 and CM2.1 models is a maximum in northern polar latitudes during late fall and winter due to the sea ice and mixed layer interactions (Manabe and Stouffer 1979) and in spring due to the reductions in snow cover (Fig. 6a). The SAT change is a minimum during the summer season over the Arctic because SAT is near freezing due to surface melting during the summer season. The lower-latitude changes are smaller and have a smaller seasonal variation. Again, this pattern of mean state changes has been shown by previous authors (see Manabe et al. 1991; Cubasch et al. 2001).

The corresponding seasonal analysis of variance change indicates that the variance decreases in northern polar latitudes during fall, winter, and spring and increases during the summer season (Figs. 6b,c) for both models. The major decreases of variance occur at or near the sea ice edge, which changes latitudinal position throughout the year. The study by Raisanen (2002) also noted a similar pattern in the reduction of

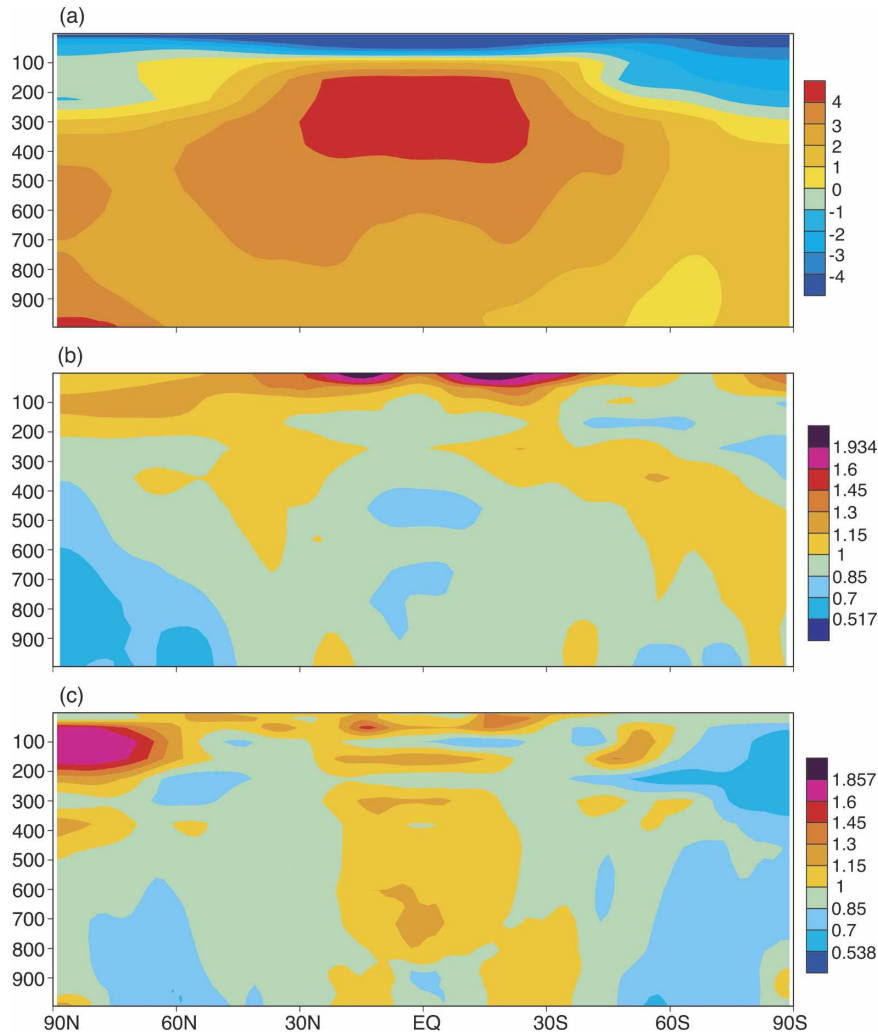


FIG. 5. Latitude–height distributions of zonal mean, annually averaged (a) CM2.1 atmospheric temperature difference in $^{\circ}\text{C}$, (b) R30 variance ratio, and (c) CM2.1 variance ratio. The variance ratios are computed by dividing the transient variance by the control variance. The zonal averages are computed from the local variance values. End-member colors indicate regions of statistical significance at the 90% confidence level. The time periods used are the same as in Fig. 1.

temperature variance during the winter season in mid- to higher latitudes.

There are two regions of statistical significance at the 90% level in high latitudes during late spring and also during the early fall. For CM2.1 (Fig. 6c), only early fall, high-latitude locations show statistically significant variance changes. The CM2.1 late spring, high-latitude variance changes are nearly statistically significant at the 90% level. In the southern polar region, there are no statistically significant variance changes, consistent with the smaller response in this region.

In the NH summer, the SAT variance increases over mid- to higher latitudes. This is especially true for

CM2.1. It is, therefore, worthwhile to briefly discuss the seasonal geographical changes of SAT variance.

The mean seasonal SAT changes have been previously published (e.g., Manabe and Wetherald 1987; Manabe et al. 1992; Cubasch et al. 2001), here we focus on the SAT variance changes. The decrease in wintertime SAT variability (Figs. 7a,c for the NH and Figs. 7b,d for the SH) in regions where the sea ice margin retreated is again seen (see discussion above).

An additional feature present over the mid- and high latitude NH continents for the June–August (JJA) plots (Figs. 7b,d) is the increased SAT variance in these regions. These increases suggest an increased frequency

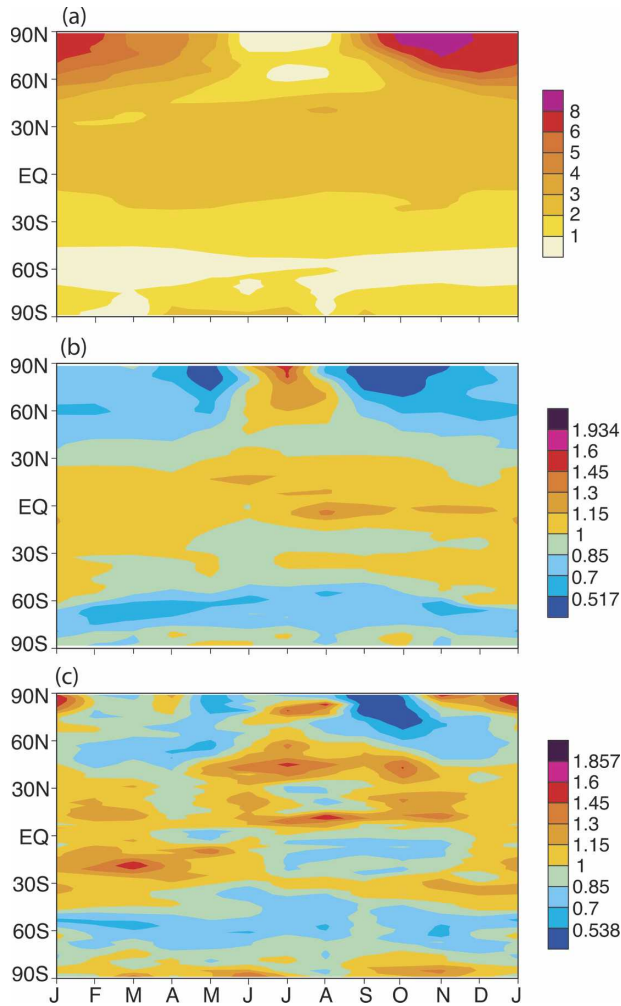


FIG. 6. Latitude–time distribution of zonally averaged SAT (a) CM2.1 mean difference in $^{\circ}\text{C}$, (b) R30 variance ratio, and (c) CM2.1 variance ratio. The time periods used are the same as in Fig. 1. Here the local mean and variance changes are zonally averaged for each month. The variance ratios are computed by dividing the transient variance by the control variance. End-member colors indicate regions of statistical significance at the 90% confidence level.

of warm or hot spells (heat waves) during the NH summer season. It is important to remember that the variance is computed about a warming mean climate (see the appendix), so that the extremes are much warmer than the extremes found in the control integration. Over North America and Europe in the CM2.1 results (Fig. 7d), there is a maximum of SAT variance increase. To a lesser extent, SAT variance increases are evident over most of North America for the R30 model as well (Fig. 7b). An analysis of the corresponding mean SAT differences (not shown) indicated that these midlatitude land regions of variance increase are places where the mean SAT increase is largest.

Meehl and Tebaldi (2004) concluded that more intense, frequent, and longer-lasting heat waves could occur in the latter half of the twenty-first century over the United States and Europe due to global warming. The results present here are consistent with their conclusions. In addition, the regions of SAT mean and variance increase are also regions of maximum soil moisture decrease, a topic that will be explored more fully in a companion paper.

During December–February (DJF), the variance decreases in the Bering Sea found in both models are statistically significant at the 90% level. Variance changes southeast of Greenland for the R30 model and off the northwestern coast of Europe for CM2.1 are also significant at this confidence level. Again, these are regions where the lower boundary of the atmosphere is changing: sea ice–covered to open ocean (Figs. 1b,d). For JJA, aside from many small regions in the Tropics involving positive variance increases, statistical significance is noted in CM2.1 for the eastern portion of the U.S. and western Europe in the midlatitudes. The same is not true for the R30 model where the mean changes (and associated variance changes) are considerably smaller.

Although the reduction of high-latitude variance has been attributed to reductions in the seasonal boundaries of sea ice, it is possible that changes of wind variance (an indicator of storminess) can also contribute to this reduction. To examine this possibility, we computed the monthly changes in surface wind speed and its variance changes as a surrogate for the storminess changes for both models (Fig. 8).

There are generally small changes of surface mean wind speed over most of the NH for the R30 model (Fig. 8a). However, there are more significant changes in the SH that mainly consist of a decrease centered at 40°S and an increase centered at 60°S . Additional analysis indicates that this shift in the winds extends to the top of the model atmosphere and is therefore attributable to both a southward shift and an increase of the wind maximum in the SH due to greenhouse warming. This feature was also found in an earlier study using the R30 model (Kushner et al. 2001), in the Canadian Climate Model (Fyfe et al. 1999), and in Cubasch et al. (2001).

There is a reduction of wind variance in mid- to higher latitudes during the NH winter followed by an increase during early spring for the R30 model (Fig. 8b). However, this feature is absent in the CM2.1 variance changes (Fig. 8c). We found very little relationship

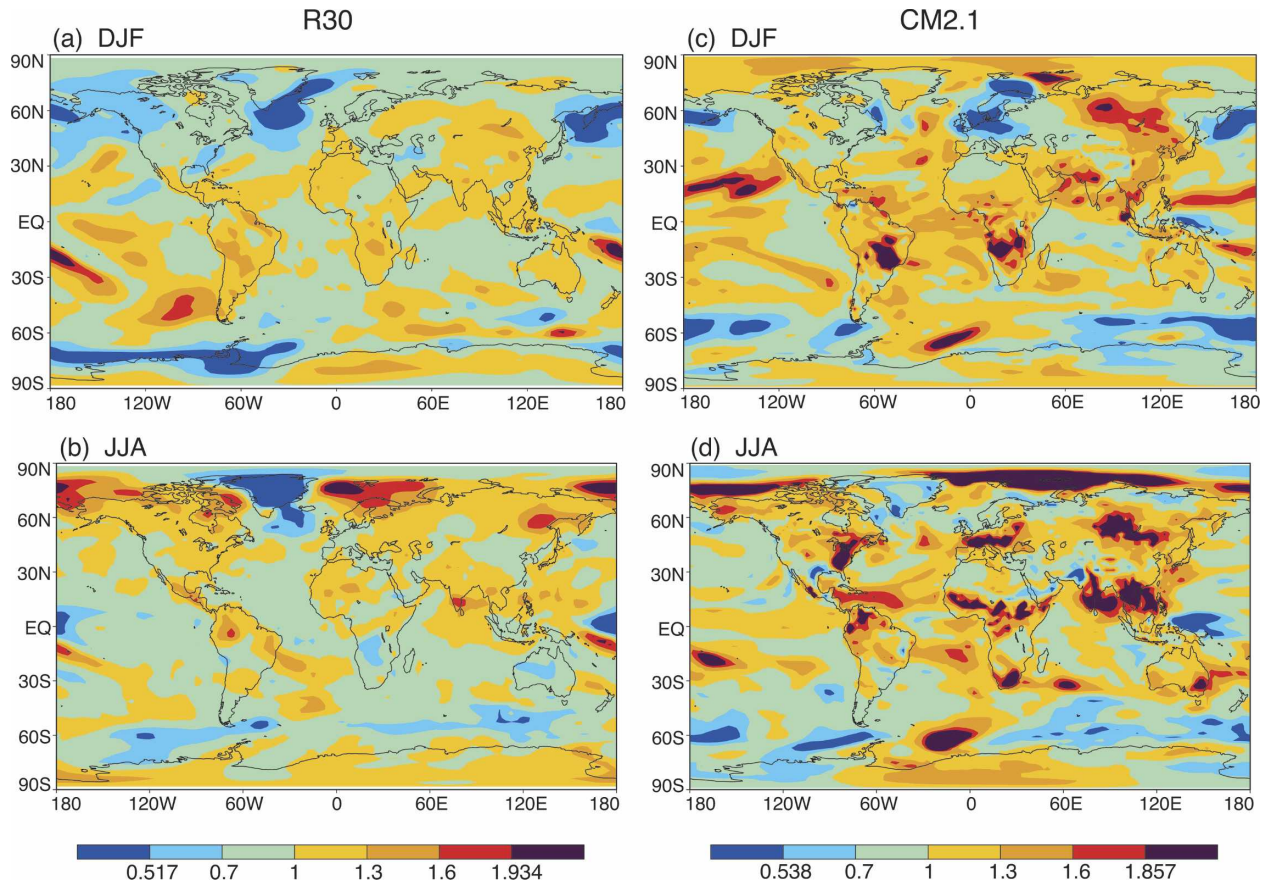


FIG. 7. Horizontal distribution of seasonally averaged SAT variance ratios: (a) DJF and (b) JJA for R30; (c) DJF and (d) JJA for CM2.1. Here the variances are computed for each model ensemble member and averaged. The variance ratios are computed by dividing the transient variance by the control variance. End-member colors indicate regions of statistical significance at the 90% confidence level. Averaging periods are the same as in Fig. 1.

between the pattern of the changes of SAT and surface wind variance. In addition, the percentage changes in variance of wind variance are relatively small. This suggests that the change in storminess and associated wind variance is not the major factor in causing the large-scale reduction of the SAT variance in high latitudes, although we cannot rule out that storminess changes are an important factor locally for some months. Therefore, it appears likely that the reduction of the sea ice margin/thickness is the major cause of the year-round decrease in SAT variance in higher polar latitudes.

Mearns et al. (1995) found a similar pattern of seasonal surface air temperature variance changes to that shown above. In their study, the changes in daily and diurnal temperature variance were analyzed. Here we use monthly and annually averaged temperature data. However, despite these differences, the temperature variance changes presented here are very similar to those reported in the Mearns et al. study.

4. Summary and conclusions

We investigated the changes in variability of temperature for two different versions of the Geophysical Fluid Dynamics Laboratory (GFDL) coupled models: an older R30 model and the newer CM2.1 model in response to the IS92a and SRES A1B scenarios, respectively. An ensemble of 8 integrations using the R30 model results and 10 using the CM2.1 model results is analyzed. As noted in the introduction, past studies of variability changes in response to increases in GHG have, for the most part, been focused on limited regions or specific phenomena whereas the current investigation is more global in scope and is designed to estimate possible changes in climate variability over extended regions. We used a simple but an unambiguous method for computing means and variance proposed by Vinnikov and Robock because it cleanly separates the mean and trends of the mean from the variance and trend in the variance in a consistent fashion. Monthly and an-

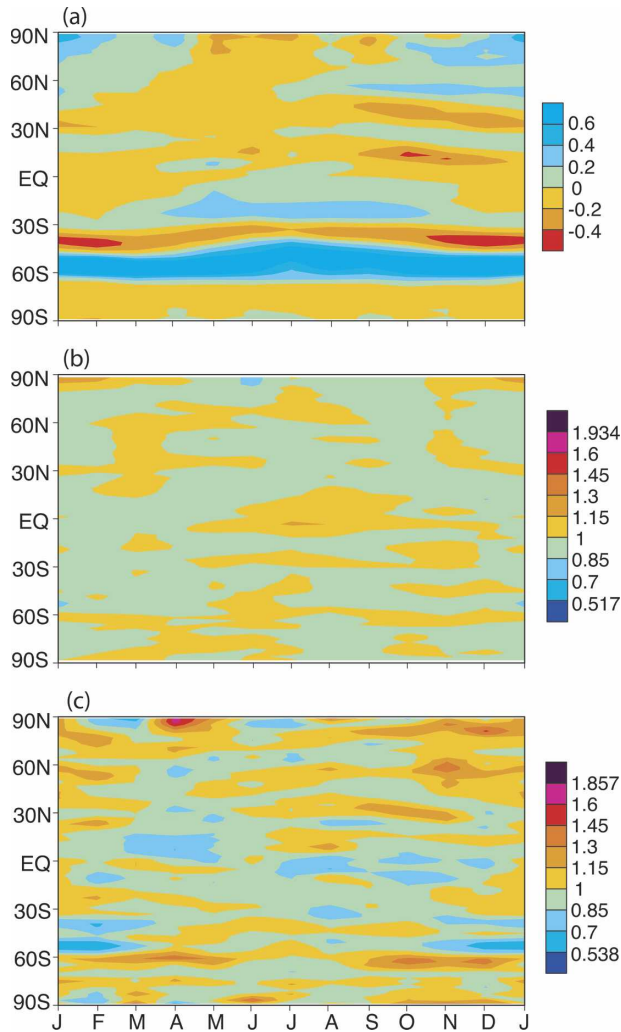


FIG. 8. Latitude–time distribution of zonal mean surface wind speed (a) CM2.1 difference in m s^{-1} , (b) R30 variance ratio, and (c) CM2.1 variance ratio. The variance ratios are computed by dividing the transient variance by the control variance. End-member colors indicate regions of statistical significance at the 90% confidence level. The time periods used are the same as in Fig. 4.

nual mean temperature data are analyzed. The analysis is focused on the changes in the variance during the middle of the twenty-first century as compared to a preindustrial control.

In general, it was found that the large-scale variance change of lower-tropospheric temperature (including surface air temperature) was reduced in mid- to higher latitudes of the NH during the fall, winter, and spring, due to reductions in the sea ice thickness and the sea ice margin retreating poleward. These reductions in sea ice cause the surface to behave more like open ocean rather than a land surface, which, in turn, reduces the surface temperature variability due to its greater heat

capacity. Smaller reductions of variance were noted around the edge of the Antarctic continent, which are also associated with sea ice retreat. Elsewhere, small variance changes occurred that are not consistent from one model to another or even among ensemble members using the same model. Small increases in SAT variance in the NH occurred from the mid- to high latitudes during the summer season. The combination of increasing mean SAT and its variance over NH land areas suggests the possibility of more frequent and longer-lasting heat waves as the planet warms in response to increase GHG in the atmosphere. The corresponding hydrologic changes will be discussed in a companion paper.

Although this study is conducted with two completely different versions of a climate model and 18 different transient integrations, we feel that the results are still tentative at this point. The analysis shown here is centered on the middle of this century. If we were able to perform this analysis on longer integrations, it is likely that the variance changes would have been larger and more statistically significant. Also the statistical significance is reduced, because we chose a conservative estimate for the number of degrees of freedom. This choice, along with the relatively small number of integrations, leads to only a small number of areas being statistically significant in this investigation.

Additional investigations need to be performed with different coupled models to provide a more definitive evaluation of variance change of climate caused by GHG forcing. However, the high-latitude large-scale patterns of variance change appear to be reasonably consistent among the integrations presented here and related to robust changes in the mean climate (i.e., the sea ice edge retreat); this provides us with confidence in the credibility of the signs of the computed variance changes.

Acknowledgments. The authors thank Konstantin Vinnikov for his assistance in applying his analysis scheme to our model results. The authors wish to thank Suki Manabe for his leadership in producing the R30 MCM runs and for his pioneering work on which many of the results presented here stand. The authors also wish to thank Tom Delworth, Keith Dixon, and Tom Knutson for setting up and integrating the experiments for the R30 model and Michael Spelman for his excellent assistance in extending the experiments run by Fanrong Zeng for the CM2.1 model. Finally, thanks are given to Joseph Sirutis, Michael Winton, Elena Shevliakova, Mike Spelman, Jerry Meehl, Ants Leetmaa, and two anonymous reviewers for reviewing the manuscript and giving many helpful suggestions.

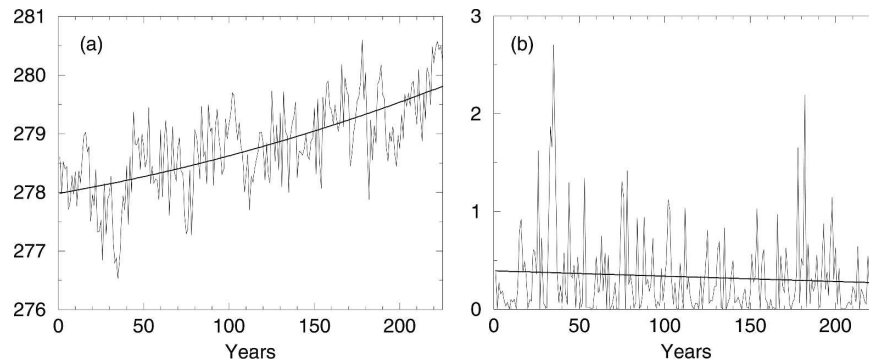


FIG. A1. Annually averaged SAT taken from a single grid point located at 59°N , 30°W . The (a) original time series (thin line) together with quadratic fit using Eq. (1) (thick line) and (b) time series of variances (thin line) computed by method of Vinnikov and Robock (2002) together with the linear fit (thick line). Units are in (a) K and (b) K^2 . The grid point is located in the oceanic region of sea ice reduction southeast of Greenland for one of the R30 model ensemble members and was chosen to, again, highlight the reduction of temperature variance noted in this study.

APPENDIX

Computation of Variance

The VR method proposed by Vinnikov and Robock (2002) may be outlined as follows. Using the VR scheme and terminology, let $y(t)$, $t = t_1, t_2, t_3, \dots, t_n$ be a time series of annual averages of some climate variable y and let t be the year number [in this example, $y(t)$ is the annually averaged precipitation rate]. Assuming that the expected value, $E[y(t)]$ may be defined by a quadratic curve, we have

$$Y1(t) = E[y(t)] = a_1 + b_1t + c_1t^2. \quad (\text{A1})$$

The coefficients a_1 , b_1 , and c_1 may be estimated by a standard least squares technique (i.e., Press et al. 1989). Once this is done, the perturbations about this quadratic curve may be computed using Eq. (A2):

$$y'(t) = y(t) - Y1(t) = y(t) - a_1 - b_1t - c_1t^2. \quad (\text{A2})$$

The variances are obtained as the anomalies about the quadratic curve $[y'(t)]^2$ for each point in the time series. The trend in the variance time series is simply a fit with a straight line of the form:

$$Y2(t) = a_2 + b_2t. \quad (\text{A3})$$

Again, the coefficients a_2 and b_2 are evaluated using a least squares technique (Press et al. 1989). This latter quantity, b_2 or the slope of the line, together with $y'(t)^2$ will form the basis for the analysis presented in this paper. Therefore, b_2 represents the trend of the variances.

The VR method has the desirable features that 1) it takes into account the fact that the mean state is chang-

ing throughout the transient experiments and 2) it provides a unique, unambiguous time series of variances once the order of the polynomial to remove the mean is determined. A schematic of this method of analysis is shown in Figs. A1a,b. Fig. A1a shows the original time series with the quadratic mean curve fitted to the data from which the anomalies $[y'(t)]$ are computed. Figure. A1b shows the resulting time series of variances computed from the information in Fig. A1a along with the linear curve fitted to the variance time series.

As noted above, the only unknown parameter in the VR method is the degree of the polynomial used to remove the trend. K. Y. Vinnikov (2004, personal communication) has indicated that, for most variables over the historical record, only a second-order (or quadratic) polynomial is necessary to estimate the changes in the mean state. To test this conclusion, we recalculated several of the fields shown in this paper using a third-order polynomial. It was found that the variance changes were almost identical to the ones obtained from using the second-order polynomial. Based upon this analysis, we decided to use the VR method with a second-order polynomial in the results presented throughout this paper.

REFERENCES

- Cubasch, U. G., and Coauthors, 2001: Projections of future climate change. *Climate Change 2001: The Scientific Basis*, J. T. Houghton et al., Eds., Cambridge University Press, 525–582.
- Delworth, T. L., R. J. Stouffer, K. W. Dixon, M. J. Spelman, T. R. Knutson, A. J. Broccoli, P. J. Kushner, and R. T. Wetherald, 2002: Review of simulations of climate variability and change with the GFDL R30 coupled climate model. *Climate Dyn.*, **19**, 555–574.

- , and Coauthors, 2006: GFDL's CM2 global coupled climate models. Part I: Formulation and simulation characteristics. *J. Climate*, **19**, 643–674.
- Fyfe, J. C., G. J. Boer, and G. M. Flato, 1999: The Arctic and Antarctic Oscillations and their projected changes under global warming. *Geophys. Res. Lett.*, **26**, 1601–1604.
- Houghton, J. T., G. J. Jenkins, and J. J. Ephraums, Eds., 1990: *Climate Change: The IPCC Scientific Assessment*. Cambridge University Press, 365 pp.
- , L. G. Meira Filho, B. A. Callander, N. Harris, A. Kattenberg, and K. Maskell, Eds., 1996: *Climate Change 1995: The Science of Climate Change*. Cambridge University Press, 572 pp.
- , Y. Ding, D. J. Griggs, M. Noguer, P. J. van der Linden, X. Dai, K. Maskell, and C. A. Johnson, Eds., 2001: *Climate Change 2001: The Scientific Basis*. Cambridge University Press, 881 pp.
- Hunt, B. G., and T. I. Elliot, 2004: Interaction of climatic variability with climate change. *Atmos.–Ocean*, **42**, 145–172.
- Katz, R. W., and B. G. Brown, 1992: Extreme events in a changing climate: Variability is more important than averages. *Climatic Change*, **21**, 289–302.
- Kharin, V. V., and F. W. Zwiers, 2005: Estimating extremes in transient climate change simulations. *J. Climate*, **18**, 1156–1173.
- Kushner, P. J., I. M. Held, and T. L. Delworth, 2001: Southern Hemisphere atmosphere circulation response to global warming. *J. Climate*, **14**, 2238–2249.
- Manabe, S., 1969: Climate and the ocean circulation. 1. The atmospheric circulation and the hydrology of the earth's surface. *Mon. Wea. Rev.*, **97**, 739–774.
- , and R. T. Wetherald, 1975: The effects of doubling the CO₂ concentration on the climate of a general circulation model. *J. Atmos. Sci.*, **32**, 3–15.
- , and R. J. Stouffer, 1979: A CO₂-climate sensitivity study with a mathematical model of the global climate. *Nature*, **282**, 491–493.
- , and R. T. Wetherald, 1980: On the distribution of climate change resulting from an increase in CO₂ content of the atmosphere. *J. Atmos. Sci.*, **37**, 99–118.
- , and —, 1987: Large-scale changes of soil wetness induced by an increase in atmospheric carbon dioxide. *J. Atmos. Sci.*, **44**, 1211–1255.
- , R. J. Stouffer, M. J. Spelman, and K. Bryan, 1991: Transient response of a coupled ocean–atmosphere model to a gradual change of atmospheric CO₂. Part I: Annual mean response. *J. Climate*, **4**, 785–818.
- , M. J. Spelman, and R. J. Stouffer, 1992: Transient response of a coupled ocean–atmosphere model to a gradual change of atmospheric CO₂. Part II: Seasonal response. *J. Climate*, **5**, 105–126.
- Mearns, L. O., 1993: Implications of global warming for climate variability and the occurrence of extreme climate events. *Drought and Assessment Management and Planning: Theory and Case Studies*, D. A. Wilhite, Ed., Kluwer, 109–130.
- , F. Giorgi, I. McDonald, and C. Shields, 1995: Analysis of variability and diurnal range of daily temperature in a nested regional climate model: Comparison with observations and doubled CO₂. *Climate Dyn.*, **11**, 193–209.
- Meehl, G. A., and C. Tebaldi, 2004: More intense, more frequent, and longer lasting heat waves in the 21st century. *Science*, **305**, 994–997.
- , H. Teng, and G. W. Branstator, 2006: Future changes of El Niño in two global coupled climate models. *Climate Dyn.*, **26**, 549–566.
- Milly, P. C. D., and A. B. Shmakin, 2002: Global modeling of land water and energy balances. Part I: The land dynamics (LaD) model. *J. Hydrometeorol.*, **3**, 283–299.
- Moorthi, S., and M. J. Suarez, 1992: Relaxed Arakawa–Schubert: A parameterization of moist convection for general circulation models. *Mon. Wea. Rev.*, **120**, 978–1002.
- Nakicenovic, N., and Coauthors, 2000: *IPCC Special Report on Emissions Scenarios*. Cambridge University Press, 599 pp.
- Press, W. H., B. P. Flannery, S. A. Teukolsky, and W. T. Vetterling, 1989: *Numerical Recipes: The Art of Scientific Computing*. Cambridge University Press, 702 pp.
- Raisanen, J., 2002: CO₂-induced changes in interannual temperature and precipitation variability in 19 CMIP2 experiments. *J. Climate*, **15**, 2395–2411.
- Rind, D., R. Goldberg, and R. Ruedy, 1989: Change in climate variability in the 21st century. *Climatic Change*, **14**, 5–38.
- Rotstain, L. D., 1997: A physically based scheme for the treatment of stratiform clouds and precipitation in large-scale models. I: Description and evaluation of microphysical processes. *Quart. J. Roy. Meteor. Soc.*, **123**, 1227–1282.
- Russell, J. L., R. J. Stouffer, and K. W. Dixon, 2006: Intercomparison of the Southern Ocean circulations in IPCC coupled model control simulations. *J. Climate*, **19**, 4560–4575.
- Stouffer, R. J., 2004: Time scales of climate response. *J. Climate*, **17**, 209–217.
- , A. J. Weaver, and M. Eby, 2004: A method for obtaining initial conditions for use in climate change studies. *Climate Dyn.*, **23**, 327–339.
- , and Coauthors, 2006a: GFDL's CM2 global coupled climate models. Part IV: Idealized climate response. *J. Climate*, **19**, 723–740.
- , J. R. Russell, and M. J. Spelman, 2006b: Importance of oceanic heat uptake in transient climate change. *Geophys. Res. Lett.*, **33**, L17704, doi:10.1029/2006GL027242.
- Tiedtke, M., 1993: Representation of clouds in large-scale models. *Mon. Wea. Rev.*, **121**, 3040–3061.
- Vinnikov, K. Y., and A. Robock, 2002: Trends in moments of climate indices. *Geophys. Res. Lett.*, **29**, 141–144.
- Wetherald, R. T., and S. Manabe, 2002: Simulation of hydrologic changes associated with global warming. *J. Geophys. Res.*, **107**, 4379–4394.
- Zwiers, F. W., and V. V. Kharin, 1998: Changes in the extremes of the climate simulated by CCC GCM2 under CO₂ doubling. *J. Climate*, **11**, 2200–2222.